Renewable Energy 163 (2021) 198–212

Contents lists available at ScienceDirect

Renewable Energy

journal homepage: www.elsevier.com/locate/renene

Energy assessment based on semi-dynamic modelling of a photovoltaic driven vapour compression chiller using phase change materials for cold energy storage

Efstratios Varvagiannis [a, *], Antonios Charalampidis [a], Gabriel Zsembinszki [b], Sotirios Karellas [a], Luisa F. Cabeza [b]

[a] National Technical University of Athens, Heroon Polytechniou 9, 15780, Zografos, Greece
[b] GREiA Research Group, INSPIRES Research Centre, Universitat de Lleida, Pere de Cabrera s/n, 25001, Lleida, Spain

ARTICLE INFO

Article history:
Received 18 January 2020
Received in revised form
27 July 2020
Accepted 10 August 2020
Available online 21 August 2020

Keywords:
Photovoltaics
Vapour compression chiller
Phase change materials
Semi-dynamic modelling

ABSTRACT

Solar cooling systems are a promising solution for reducing the electrical consumption of conventional building cooling systems. Among various alternatives, photovoltaic driven vapour compression chillers are currently the most mature and economically feasible solar cooling technology. This study focuses on the semi-dynamic modelling of a vapour compression chiller coupled with a novel refrigerant-phase change material (PCM)-water heat exchanger (RPW-HEX) which replaces the conventional chiller's evaporator, allowing the efficient storage of the produced cooling energy. A custom-build lumped parameter model was developed in TRNSYS and was used to assess the performance of the proposed system on annual basis. Using as benchmark a conventional PV driven vapour compression chiller with electrical storage, the retrofitted hybrid storage system showed improved performance, limiting the cooling demand peaks and enhancing the solar fraction, especially for partial cooling loads. Last, a comparison of the PCM thermal energy storage to conventional batteries was carried out, leading to enhanced performance characteristics for the latter.

1. Introduction

Reducing the energy consumption for domestic cooling and heating is a major goal for the EU, as it is indicated by the short term 2020 goals [1]. Currently, the residential sector has a share of 25% in the final energy consumption of the EU [2], being one of the most important energy consumption fields. As a result, enhancing the penetration of renewables is of major importance, being in consistency with the definition of nearly Zero Energy Buildings (nZEBs) [3]. In this context, utilizing solar energy for heating and cooling is possibly one of the most popular solutions, playing an important role for reaching the nZEB targets, especially for Mediterranean climates [4]. While solar heating system layouts are usually evident, for solar cooling applications either thermal (based on sorption technology) or electrical (based on photovoltaic driven vapour compression chillers) solutions are usually considered. Although no significant differences in the total investment cost for either thermal or electrical solar cooling technologies is evident in the literature [5], the extended experience and manufacturing maturity of the vapour compression technology is expected to lead to more efficient systems in terms of COP and consequently in economically more competitive solutions [6].

Another important aspect of solar cooling applications is the necessity of energy storage. Energy storage systems are required for two reasons: first, they allow the enhancement of the solar energy fraction by matching the maximum cooling demand (usually expected in the afternoon for residential air conditioning) with the peak solar energy production and, second, they reduce the operational costs, especially for countries where Net Metering Policy is applied for photovoltaic electricity. In solar driven cooling systems, the use of battery banks is the most common storage solution, but use of sensible and latent thermal energy storage is also an option. Beck et al. [7] focused on a domestic refrigerator powered by PV, with two levels of cold storage using PCM (for the refrigerator and the freezer respectively), pointing out that depending on the retail price of electricity, the thermal energy storage solution can be economically more competitive than the no storage solution and

* Corresponding author.
E-mail address: svarv@mail.ntua.gr (E. Varvagiannis).

https://doi.org/10.1016/j.renene.2020.08.034

always better than the battery storage. Wu et al. [8] verified experimentally a PV driven vapour compression chiller for domestic cooling, combining both batteries and ice thermal energy storage, which was implemented by using a water tank into which the evaporator of the chiller was immersed. They concluded that the system could operate autonomously even without the electrical storage. Wang et al. [9] simulated in TRNSYS a heat pump driven compression chiller with low temperature thermal energy storage considering three different PCM (including ice), focusing on the comparison between the battery and the thermal energy storage in terms of grid electricity consumption and primary energy savings. In any case, they noticed enhanced primary energy savings in the scenarios were either electrical or thermal energy storage was utilized. In addition, thermal energy storage was associated with higher electricity consumptions, primarily due to the lower set point temperatures needed for storage charging, which lead to worse values for the chiller COP. Last, although the ice storage was inferior in terms of specific storage capacity, it suffered from increased thermal losses and worse performance due the low storage temperature level.

In this study a PV driven water cooled chiller, modified to operate with a novel refrigerant-PCM-water heat exchanger (RPW-HEX) as evaporator, is the heart of the proposed domestic cooling system. Electrical storage (batteries) and low temperature energy storage (LTES), implemented using paraffin PCM with 4 °C melting temperature, are combined in order to maximize the solar fraction. Cooling energy produced by the compression chiller can be simultaneously stored to the PCM and/or transferred to the heat transfer fluid (HTF) and flow through the cooling emission system of the building, the latter consisting of conventional fan coil units (FCU). Besides, a standard DC/AC converter is used in order to connect the PV-batteries electrical subsystem to the building AC grid and to monitor the electrical energy required from the electrical grid. In case of low cooling demand, the produced electricity from PV can either be stored in the hybrid storage solutions, or be dumped (actually fed back to the electrical grid, but without any economic benefit). As a result, excess electricity is not considered as beneficial, similarly to the Net Metering policy, which is applied in many European countries (including Greece).

In fact, the aforementioned system is part of a more complicated layout, which is being developed within the context of the H2020 research project HYBUILD. The HYBUILD system consists of two different options, one for Continental and one Mediterranean climates. The latter one, designed especially for cooling purposes, incorporates three different energy storage options: (a) electrical batteries, used for PV electricity storage, (b) low temperature thermal energy storage using PCMs, aiming to directly cover space cooling demands, and (c) a sorption chiller, driven by thermal solar collectors, which cools down the condenser of the vapour compression chiller and potentially acts as medium temperature thermal energy storage for domestic hot water (DHW) production. Contrary to the system considered in the present study, the electrical components of the original HYBUILD system (compression chiller, PV, and batteries) are directly connected to a DC grid, in order to eliminate conversion losses.

Fig. 1 shows both the studied subsystem and the full system of the project HYBUILD. Only the components with dashed borderlines were considered in this study, while the rest of the components are part just of the HYBUILD Mediterranean layout.

The present study aims to develop a simplified, yet accurate, semi-dynamic model of the integrated vapour compression chiller with RPW-HEX subsystem, ideal for control simulations and annual system assessment with low computational cost. A lumped parameter approach using an equivalent 3R–1C thermal network (see Fig. 2) was followed. Similar approaches for simplified PCM tank models were already implemented in a variety of relevant previous studies, as for example in Refs. [10,11]. The model is written in C++ and linked to TRNSYS simulation software. Using

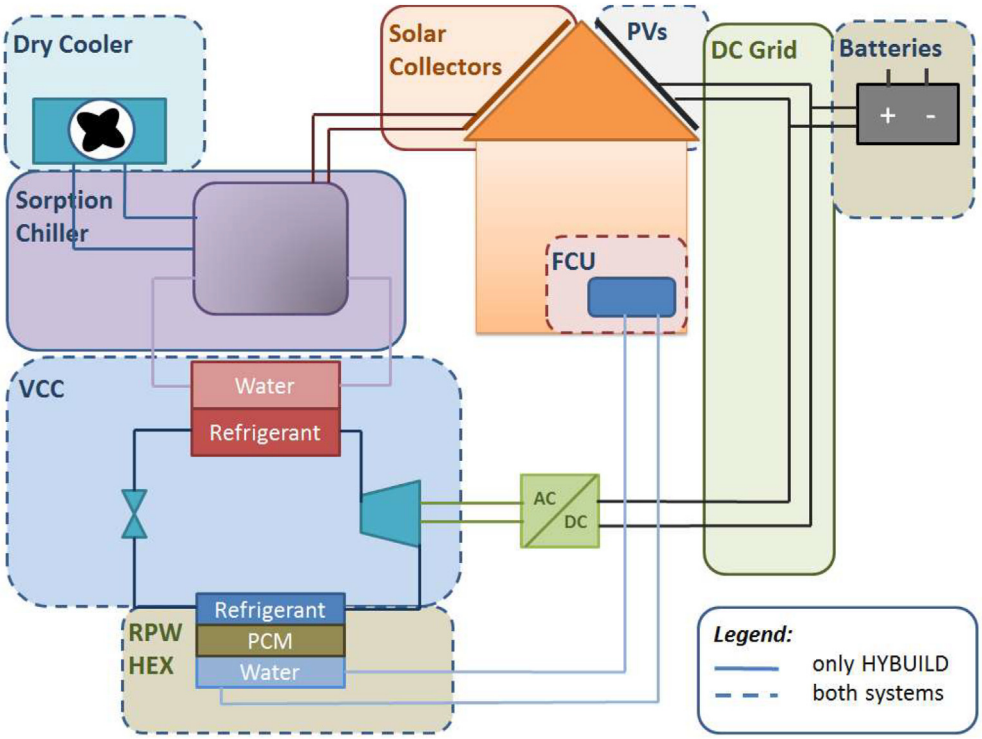

Fig. 1. Schematic representation of the overall HYBUILD system and the subsystem examined in the present study.

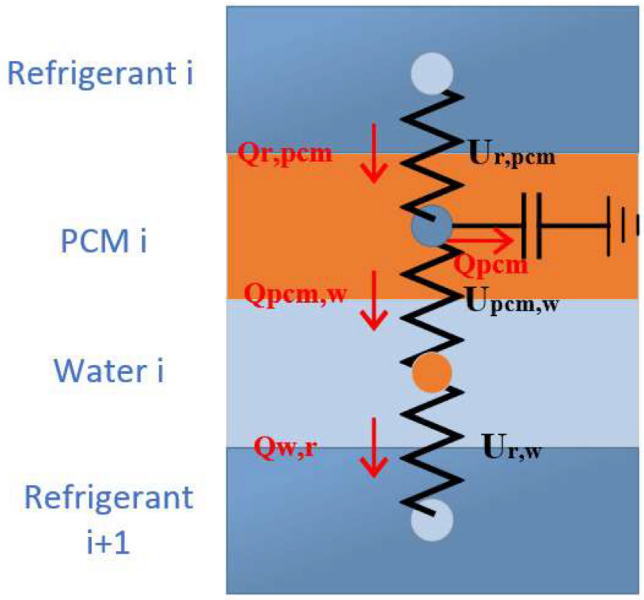

Fig. 2. Schematic representation of the 3R–1C lumped parameter model of the RPW-HEX.

the aforementioned model, the performance of the hybrid electrical/thermal energy storage solution in terms of grid energy consumption (GEC) and solar fraction (SF) is compared to a conventional PV cooling system with only electrical storage, utilizing standard components available in TRNSYS libraries for the rest of the components.

2. Modelling methodology

2.1. Modelling of the vapour compression chiller

The vapour compression chiller was modelled with static performance correlations [12] generated from data provided by the chiller manufacturer. These expressions allow the calculation of the scaled evaporator cooling capacity $Q^*_{evap} = Q_{evap}/Q_{evap_{nom}}$ and the thermal energy consumption of the compressor $Q^*_{comp} = Q_{comp}/Q_{comp_{nom}}$ as a function of the scaled evaporation pressure $x^* = p_{evap}/p_{evap_{nom}}$, and the scaled condenser inlet water temperature $y^* = T_{wc,in}/T_{wc,in_{nom}}$. In any case, the subscript nom indicates the value of the respective variable for the nominal conditions defined by the chiller manufacturer, being available in Table 1 below.

$$Q^*_{evap} = -92.54 + 204.9 \cdot x^* - 96.52 \cdot x^{*2} + 76.71 \cdot y^* - 34.71 \cdot y^{*2} - 164.1 \cdot x^* \cdot y^* + 85.85 \cdot x^{*2} \cdot y^* + 73.47 \cdot x^* \cdot y^* - 40.25 \cdot x^{*2} \cdot y^{*2} \quad (1)$$

$$Q^*_{comp} = -5.437 + 13.68 \cdot x^* - 7.849 \cdot x^{*2} + 4.544 \cdot y^* - 0.6074 \cdot y^{*2} - 6.721 \cdot x^* \cdot y^* + 4.472 \cdot x^{*2} \cdot y^* + 1.145 \cdot x^* \cdot y^* - 0.7342 \cdot x^{*2} \cdot y^{*2} \quad (2)$$

Using the above expressions, and given the nominal values for each variable as model parameters, the following can be directly calculated:

$$Q_{cond} = Q_{evap} + Q_{comp} \quad (3)$$

$$P_{comp} = \frac{Q_{comp}}{e_{mot}} \quad (4)$$

$$COP = \frac{Q_{evap}}{P_{comp}} \quad (5)$$

where e_{mot} is the motor efficiency and is given as a model parameter as well.

In addition, given the water flow rate through the condenser, the condenser outlet temperature of the water can be also expressed as:

$$T_{wc_{out}} = T_{wc_{in}} + \frac{Q_{cond}}{m_{wc} \cdot c_{pw}} \quad (6)$$

In case that the standard evaporator of the chiller is used, the outlet temperature of the water can be calculated using a similar steady state expression:

$$T_{we_{out}} = T_{we_{in}} - \frac{Q_{evap}}{m_{wc} \cdot c_{pw}} \quad (7)$$

Since Q_{evap} is a function of the evaporation pressure (equivalently the evaporation temperature T_{evap}), an iterative procedure, based on the ε-NTU method for the standard evaporator, is needed:

Table 1
Simulation parameters for the custom vapour compression chiller RPW-HEX integrated model.

Description	Symbol	Units	Value
Convection coeff. for water flow	h_w	W/m^{2}K	850
Convection coeff. for refrigerant flow	h_r	W/m^{2}K	4500
Conductivity of PCM (defined after experimental validation of the RPW-HEX)	λ_{pcm}	W/mK	1.8
Thickness of PCM layer	d	m	0.01
Area of RPW HEX	A	m^2	18.5
Water specific heat	c_p	J/kgK	4190
Heat pump's motor efficiency	e_{mot}	–	0.93
Nominal evaporator capacity	$Q_{evap,nom}$	W	13200
Nominal compressor abs. heat	$Q_{comp,nom}$	W	3000
Nominal evap. Pressure	$p_{evap,nom}$	Pa	940000
Water Mass inside the RPW HEX	M_w	Kg	10

$$NTU_{std} = \frac{U_{std} \cdot A_{std}}{m_{we} \cdot c_{pw}} \tag{8}$$

$$\varepsilon_{std} = 1 - \exp(NTU_{std}) \tag{9}$$

$$T_{evap} = T_{we_{in}} - \frac{Q_{evap}}{\varepsilon_{std} m_{we} c_{pw}} \tag{10}$$

where $Q_{pcm,t}$ is the total heat flow from the PCM (actually >0 when the PCM is cooled down), which is the sum of the cooling flow from the refrigerant and the water nodes respectively:

$$Q_{pcm} = Q_{w \to pcm} + Q_{r \to pcm} \tag{12}$$

Besides, the thermal capacitance of the PCM was considered with a piecewise polynomial expression for the PCM node temperature as function of the total stored cold energy calculated with Eq. (13):

$$T_{PCM,t} = \begin{cases} -0.003 \cdot E_{PCM,t} + 12, \ if \ E_{PCM,t} \ \leq 2032.8 \ kJ \\ -3 \cdot 10^{-9} \cdot E_{PCM,t}^2 - 5 \cdot 10^{-5} \cdot E_{PCM,t} + 6.1087, \ if \ 2032.8 \ kJ < E_{PCM,t} < 24393.6 \ kJ \\ -6 \cdot 10^{-8} \cdot {E_{PCM,t}}^2 + 0.0025 \cdot E_{PCM,t} - 24.806, \ if \ E_{PCM,t} \geq 24393.6 \ kJ \end{cases} \tag{13}$$

2.2. Modelling of the refrigerant-PCM-water heat exchanger

As previously described, the novel RPW-HEX replaces the standard evaporator of the compression chiller, adding the capability to store the excess of the produced cooling to the latent storage when the cooling demand is less than the cooling capacity of the chiller. The structure of the passages of the RPW-HEX has the following sequence: Refrigerant-PCM-Water-Refrigerant etc. This sequence ensures that cooling energy is transferred to the HTF even when no cooling energy is needed to be stored to the PCM. Each passage is modelled as a lumped component, consisting of a single temperature node, while the overall heat transfer coefficient U between two sequential nodes is calculated according the convective heat transfer coefficient of the refrigerant or the water cells and the thermal conductivity of the PCM. The thermal losses of the storage to the ambient where considered negligible, primarily due to the small period when the storage remains charged (actually due to its small capacity, the PCM storage acts mostly as a peak shaver rather than a large time scale storage).

The nominal convective heat transfer coefficients are given as parameters to the model and for the specific application they have been calculated using the Dittus-Boelter [13] correlation for the heat exchanger geometry. The values used are summarized in Table 1, along with the rest of the model parameters.

In every time step, the cold energy stored in the PCM is calculated by means of an explicit time integration scheme:

$$E_{pcm,t} = E_{pcm,t-\Delta t} + Q_{pcm,t} \cdot \Delta t \tag{11}$$

This approach practically leads to a 3R−1C equivalent thermal network for the heat exchanger model.

Once the temperature of the PCM node is known, the state of charge of the latent storage is calculated from the following expression:

$$SOC = \begin{cases} 1, \ if \ T_{PCM,t} < -2 \ ^\circ C \\ -0.0066 \cdot T_{PCM,t}^2 - 0.041 \cdot T_{PCM,t} + 0.9444, \ if \ -2 \ ^\circ C \leq T_{PCM,t} \leq 3 \ ^\circ C \\ -0.0397 \cdot T_{PCM,t}^2 + 0.1243 \cdot T_{PCM,t} + 0.746, \ if \ 3 \ ^\circ C \ \leq T_{PCM,t} < 6 \ ^\circ C \\ -0.0106 \cdot T_{PCM,t} + 0.127, \ if \ 6 \ ^\circ C \leq T_{PCM,t} \leq 12^\circ C \\ 0, \ if \ T_{PCM,t} > 12 \ ^\circ C \end{cases} \tag{14}$$

Similarly to the definition of the total heat flow from the PCM node, the total heat flows from the refrigerant and the water nodes, Q_r and Q_w, are calculated as follows:

$$Q_r = Q_{r \to w} + Q_{r \to pcm} \tag{15}$$

$$Q_w = Q_{r \to w} - Q_{w \to pcm} \tag{16}$$

As it is evident, the following equation is valid for the total cooling flows from each node:

$$Q_r = Q_{pcm} + Q_w \tag{17}$$

The cooling flows to the water node from the refrigerant and the PCM nodes respectively are calculated following the ε-NTU method:

$$NTU_i = \frac{U_{w,i} \cdot A}{m_{we} \cdot c_{pw}} \tag{18}$$

$$\varepsilon_i = 1 - \exp(NTU_i) \tag{19}$$

$$Q_{w\to i} = \varepsilon_i \cdot m_{we} \cdot c_{pw} \cdot (T_i - T_{we_{in}}) \tag{20}$$

where the subscript i denotes either the PCM or the refrigerant node ($i = r, \quad PCM$).

Finally, assuming an isothermal profile for the PCM node and a fixed superheating equal to $T_{sh} = 4.2\,^{\circ}C$ for the refrigerant node, the heat flow between the two nodes can be calculated as:

$$Q_{r\to pcm} = U_{r,pcm} \cdot A \cdot (T_{pcm} - (T_{evap} + 2.1)) \tag{21}$$

Since the design of the RPW-HEX is associated with quite large water volumes (approximately 40 L for a 10 kWh storage capacity heat exchanger), it was preferred to use a dynamic expression for the heat balance equation on the water side of the HEX. In order to avoid iterations, an upwind discretization scheme for the water control volume was used and as a result, the evaporator leaving water temperature is calculated as follows:

$$T_{we_{out},t} = \frac{\rho_w \cdot V_w \cdot c_{pw} \cdot T_{we_{out},t-\Delta t} + (c_{pw} \cdot T_{we_i} - Q_w) \cdot \Delta t}{m_{we} \cdot c_{pw} \cdot \Delta t + \rho_w \cdot V_w \cdot c_{pw}} \tag{22}$$

2.3. Development of the integrated model and definition of the operational modes

Three different operational modes can be directly identified for the integrated VCC/RPW-HEX system:

- **Operational Mode 1: Vapour compression chiller charging the latent storage:** when no space cooling is needed but there is excess production of electric power from the PV panels.
- **Operational Mode 2: HTF discharging the latent storage:** when no electrical energy is available either directly from the PV or from the batteries, but cooling is needed.
- **Operational Mode 3: Parallel operation:** when excess of PV electricity is possible and space cooling is also needed. In this case, the PCM might be charged discharged or be thermally inactive depending on the working conditions.

At this point, it is worth mentioning that for nominal water and refrigerant conditions, the evaporation temperature is slightly over the melting temperature of the PCM and as a result the PCM layer is thermally inactive. Though, in case of low inlet water temperatures in the RPW-HEX (e.g. when cooling demand is significantly low) or reduced HTF flow rates (e.g. if a variable flow system is used for the building), simultaneous charging of the PCM and cooling of the HTF is possible.

The operation of the chiller is controlled using an external on/off signal, CS_{ext}, which can be defined by the room thermostat or by a more sophisticated controller. In addition, HTF flow inside the RPW-HEX is monitored by the flow switch of the chiller, which is enabled when the flow is below a certain limit (in this model, this limit is $\dot{V}_{FS} = 0.01\ l/s$), consisting to the CS_{FS} control signal.

Even though in normal operation the chiller is supposed to operate using the RPW-HEX as evaporator, in order to allow reversibility of the system for space heating, the standard evaporator of the chiller is maintained and just bypassed when hybrid storage operation is needed. This is implemented by installing a 3-way valve on the water side and 4 solenoid valves on the refrigerant side. All of the valves are switched between two possible positions (0 for RPW-HEX and 1 for the standard evaporator) by the same control signal, CS_{sv}. This leads to the definition of one more operation mode, which corresponds to the operation of the chiller using its standard evaporator (**Operational Mode 4**).

Finally, **Operational Mode 5** indicates that neither HTF flows in the RPW-HEX nor the chiller is operating, which means that everything is at rest.

Fig. 3 summarizes the definition of the operational modes and the logical conditions for the control signals that enable each one.

Depending on the operational mode, the set of equations slightly changes, as Fig. 4 reveals.

From Fig. 4 it is clear that for Modes 3 and 4, an iterative procedure is performed in order to determine the evaporation temperature (and equivalently the pressure) in order to satisfy the heat balance. This procedure makes the model more robust while the computational cost is not that great, since it was observed that less than 10 iterations are needed for convergence for each time step. Regarding model convergence, an absolute tolerance of 10^{-3} K on evaporation temperature is set as criterion, as depicted in Fig. 4.

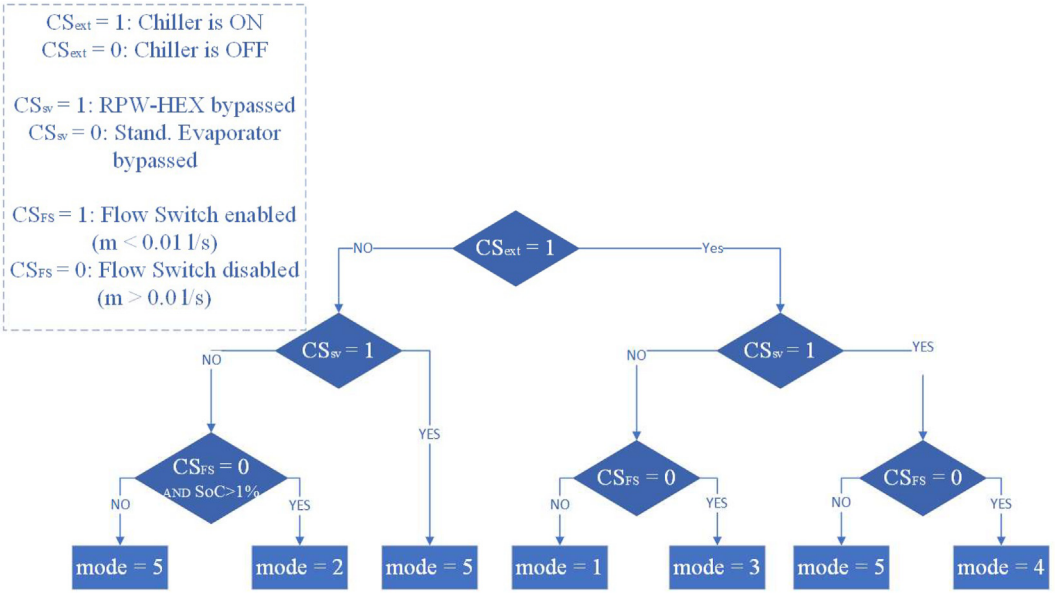

Fig. 3. Operational mode selection flow chart.

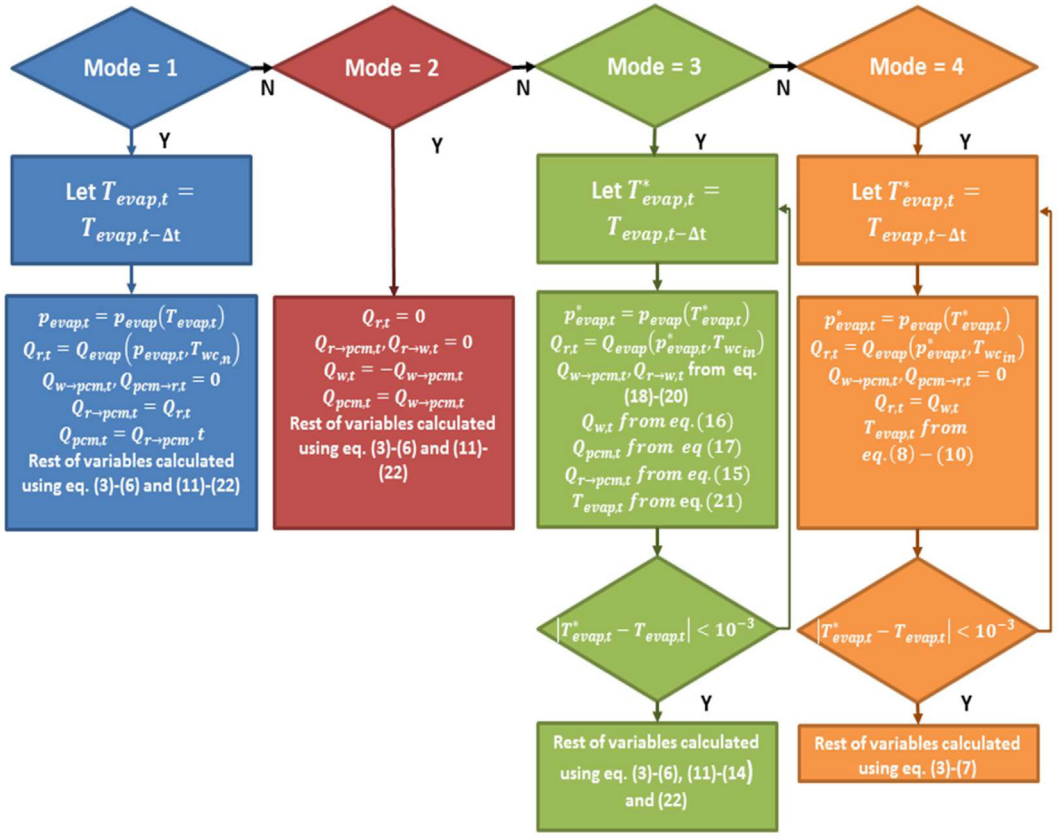

Fig. 4. Calculation procedure for the integrated vapour compression chiller RPW-HEX model as a function of the operational mode.

Table 2
Summary of the standard TRNSYS Types used for the simulation of the system.

Component	TRNSYS Type	Description
Building	88	Simplified building based on 1 lumped resistance and 1 lumped capacitance parameters
PV panels	194	Single diode PV model
Battery	47	Simple battery model based on electrical power
Grid converter	48	DC/AC converter with Net Metering and Maximum Power Point Tracking (MPPT)
Fan coil units	928	Fan coil unit with return air bypass (not used) and single fan speed
Pumps	110	Variable speed pumps

In order to ensure numerical stability −given that an explicit integration scheme was used− a small time step, less than 10 s, should be used. For compatibility with TRNSYS simulations using higher time step values, the model equations are solved internally using a time step of $\Delta t = 1\ s$, while the values returned to the TRNSYS simulation studio are the final values resulting from the component response after the end of the time step defined in TRNSYS. This means that the integration calculations are based on a 1 s time step, while the results are sampled each Δt_T seconds (where Δt_T is the TRNSYS time step) following a Zero Order Holder (ZOH) approach, while the heat flows and temperatures defined as outputs of the model are calculated as numerical average values. This method ensures stability of the whole system model, without increasing the computational cost for the simulation of static components.

2.4. Modelling of the rest of the components of the cooling system

As mentioned in the introduction, the rest of the components of the cooling system described were modelled utilizing standard components available in the TRNSYS libraries. In fact, the TRNSYS type used for each component, plus the main operational data are presented in Table 2.

Since a comparative study is performed regarding the operation of the vapour compression chiller using its standard evaporator or the RPW-HEX, it was supposed that the condenser is able to operate always at its rated performance, independently of the ambient conditions, thus no model for a dry cooler or a cooling tower was used. Even though this is obviously not realistic, it is assumed that this simplification does not affect the comparative results.

Next, a short presentation of the details and the sizing for each one of the main system component models follows. All the model parameters are summarized in each section. Fig. 5 depicts the TRNSYS simulation flow sheet.

2.5. Building model

The building model selected for the present study is based on a simple, lumped capacitance, single thermal zone model, available in TRNSYS. This implementation was considered satisfactory in

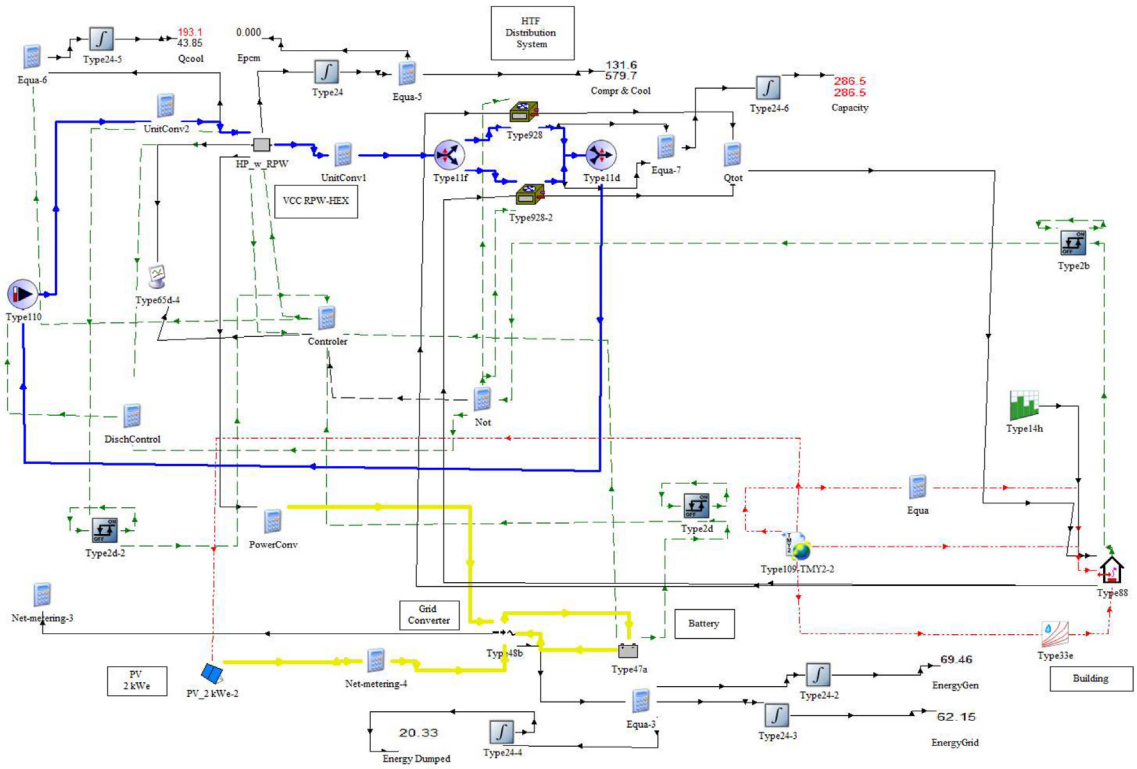

Fig. 5. The developed simulation flow sheet in TRNSYS.

Table 3
Simulation parameters for the building model.

Description	Symbol	Unit	Value
Reference Area	A_{ref}	m^2	290
Building heat loss coefficient (standard scenario)	U	W/m^2K	2
Total envelope area	A_e	m^2	540
Building heat loss coefficient (after insulation upgrade)	U′	W/m^2K	1
Lumped capacitance per m^2 of reference area	C	KJ/m^2K	150
Infiltration air flow rate per m^2 of reference area	V_{inf}	$m^3/h/m^2$	0.75
Total Glazing area	A_g	m^2	44
Solar Heat Gain Coefficient	SHGC	–	0.72
Number of living persons	$N_{persons}$	–	4

order to model the buildings behaviour and implement the thermostatic control for the energetic assessment of the system. In fact, the building heat loss coefficient and capacitance are represented by one resistive and one capacitive element, respectively. Additional thermal gains can be added to the building, including infiltration gains, gains from occupants, equipment etc. In this study, the cooling power from the FCU is added as a gain input. Besides, solar gains from glazing elements were added, as they play a major role on the determination of the cooling loads.

The modelled house typology is based on the data available from the EU research project TABULA for a typical Greek single-family house constructed in the 1980–2000 period in Athens. This typology is probably one of the most common typologies in the Greek building stock [14], while provides a good match between the expected peak cooling load and the cooling capacity of the selected vapour compression chiller. All the data for the total heat loss coefficient, capacitance, infiltration, glazing (for the calculation of solar gains) were collected from the TABULA Web Tool [15] platform and are summarized in Table 3. The thermal zone temperature control is performed by means of a differential thermostat, whose set point has the standard value of $T_{SP} = 26\ ^{\circ}C$ defined in the Greek Technical Directives [16] and a differential range of $\Delta T_{SP} = \pm 0.5\ ^{\circ}C$. If the room temperature T_{room} exceeds 26.5 °C the thermostat signal is true ($CS_{TH} = 1$), while when T_{room} drops below 25.5 °C then the thermostat signal is false ($CS_{TH} = 0$).

2.6. PV-batteries-grid converter models

As previously mentioned, the standard Type 194b from TRNSYS is used for the modelling of the PV array. This type includes the DC/DC converter that implements the MPPT algorithm, ensuring optimal operation of the panels even at no rated environmental conditions (solar irradiation, ambient temperature, etc.), while interconnection with inverter and battery models can be easily implemented. This component applies the five-parameter model [17] that includes a single diode and two resistances. The detailed modelling of the PV array is beyond the scope of this paper and is not presented hereby. As far the sizing is considered, it is noted that a typical PV module has limited rated power that does not exceed 500 W. Concerning this, in order to supply bigger electrical loads,

Table 4
Simulation paramters for the PV model.

Description	Symbol	Unit	Value
Module reference short-circuit current	I_{sc}	A	9.77
Module reference open-circuit voltage	V_{oc}	V	39.8
Module reference current at MPP	I_{mp}	A	9.19
Module reference voltage at MPP	V_{mp}	V	32.6
Reference short-circuit current temperature coefficient	μ_{sc}	A/K	0.005
Reference open-circuit voltage temperature coefficient	α_{oc}	V/K	−0.115
Module cells	N_s	–	60
Number of strings	NP	–	1
Modules per string	NS	–	10
Transmittance-absorptance product for normal incidence	$(\tau\alpha)_n$	–	0.9
Semiconductor bandgap	ε_g	eV	1.12
Cover extinction coefficient	K	m^{-1}	4
Cover thickness	L	mm	3.2
Module slope	β	deg	30
Module absorption area	A	m^2	1.47

Table 5
Simulation parameters for the battery model.

Description	Symbol	Unit	Value
Cell voltage	V_{cell}	V	2
Cell capacity	E_{oc}	Wh	120
Number of cells' strings	NP_{cell}	–	12
Cells per string	NS_{cell}	–	12
Battery voltage	V_{bat}	V	24
Charging efficiency	η_{bat}	–	0.9
Maximum SOC	SOC_{min}	–	1.0
Minimum SOC	SOC_{max}	–	0.15
SOC turning point	SOC_{tp}	–	0.25 (inactive)

Table 6
Simulation parameters for the grid converter model.

Description	Symbol	Unit	Value
Regulator rated efficiency	η_{reg}	–	0.90
Inverter rated efficiency	η_{inv}	–	0.96
Maximum input power	$P_{in,max}$	W	3500
Maximum output power	$P_{out,max}$	W	3300
Rated input voltage	$V_{inv,r}$	V	360
Minimum input voltage for MPPT operation	$V_{inv,min}$	V	170
Maximum input voltage for MPPT operation	$V_{inv,max}$	V	530
Maximum input current	$I_{inv,max}$	A	10
Night consumption	P_{night}	W	0.4

multiple modules are connected in series, constituting a string, while multiple strings are wired in parallel, forming an array. Apart from the power demand, the minimum input voltage, the maximum input voltage and the current and power specifications of the inverter, add constraints concerning the final number of strings and modules. Since these quantities are weather-dependent for the PV, the dimensioning was conducted in the worst-case scenario. More specifically, increase of cell temperature leads to increase of the current and decrease of voltage generated by the module. The minimum and maximum cell temperatures considered were −10 and 65 °C respectively. Based on this procedure, the PV array consists of a single string with ten modules of 3 kW total rated power and a total absorption area of approximately 15 m^2. The sizing was performed in order to cover the chiller demand, even in days with moderate solar irradiation (800 W/m^2), thus maximizing the solar fraction, though a techno economic evaluation of this choice is recommended as future work. Following this gross sizing procedure, the rest of the parameters for the model were obtained from specification sheets of PV manufacturers and relevant studies [18,19] and are presented in Table 4.

With regard to the batteries, a common assumption for dimensioning is that they have to provide the required stored electricity for daily self-consumption. In this study, a lead-acid battery was selected, while its capacity was estimated for approximately 40% self-sufficiency based on the figures proposed in Ref. [20] assuming an average 10 h operation per day for the cooling system throughout the cooling period, resulting in a total electrical capacity of 1.8 kWh_e. Apart from the technical specifications of the battery, its operation was determined by the fractional state of charge (SOC_b). In particular, an upper and a lower limit of SOC_b parameter were selected so that the battery does not charge above the high limit and does not discharge below the low one. Moreover, an additional SOC_b limit is defined, indicating the charge level below which priority is given to charging the battery instead of covering the load demand. The above quantities are parameters of the selected battery model and they are summarized in Table 5.

Last, the grid converter regulates the power flow between the PV, the battery and the load, taking into consideration the limitations imposed by the upper and lower battery's state of charge limits. Its rated power was selected in accordance with the PV, so that it slightly exceeds the rated power output of the PV array The performance characteristics are retrieved from a commercial model and are available in Table 6.

It is mentioned that in this study, the state of charge is measured in terms of energy (Wh) instead of amperage-hours for simplification of the modelling. Regarding this, TRNSYS Type 47a for the battery was used, in conjunction with Type 48b of the grid converter.

2.7. Fan coil units and distribution system

The cooling emission system of the building consists of two identical fan coil units (FCU), each one rated at 6.7 kW_{th} of total cooling capacity, thus matching perfectly the chiller nominal capacity. The rated fan power for each FCU is $P_{FCU} = 160\ W$ and is considered constant since speed of the fan is not controlled. It has to be mentioned that the total cooling capacity is supplied to the building as a negative thermal gain and as a result no distinction is made between sensible and latent cooling capacity, for simplicity sake.

The HTF distribution system consists of flow mixers and diverters, bad variable speed pumps, which are actually operating at their rated flow rates in almost all operating conditions except for PCM discharging (operational Mode 2) where the flow rate of the evaporator pump is set to a value equal to the half of its rated capacity, mainly in order to avoid abrupt PCM discharging and thus poor system performance, as it is better explained in the next

section. The nominal power input of the pump was $P_{pump,n} = 130\ W$, and it was assumed that it is proportional to the cubic ratio of the transferred flow rate to the nominal one, so:

$$P_{pump} = P_{pump,n}\left(\frac{m_{we}}{m_{we,n}}\right)^3 \quad (23)$$

Both the pump and the FCU electrical consumptions can be supplied by the PV system and as a result, they both were considered as an electrical load, apart from the consumption of the chiller's compressor. As result, at any time, the net supplied electrical power is the sum:

$$P_{supply} = P_{grid} + P_{PV} + P_{bat} = P_{comp} + P_{pump} + 2 \cdot P_{FCU} \quad (24)$$

2.8. Hybrid storage system control strategy

The control strategy of the whole HVAC system should be able to maintain the room temperature T_{room} within the limits imposed by the thermostat ($26 \pm 0.5^{\circ}C$), while it should maximize the utilization of solar energy.

While just the room temperature thermostat along with the grid converter are sufficient for the conventional system (which lacks of thermal energy storage capability), a more complex approach should be followed in order to make use of the thermal energy storage. First of all, it is important to mention that during nominal operation the PCM layer is practically inactive, since the evaporation temperature is higher than its melting temperature. As a result, the thermal energy storage can be charged only when no cooling is needed (operational Mode 1). Besides, the aforementioned remark means that if the thermal energy storage is fully or partially charged and cooling is needed, priority should be given to smoothly discharging it (operational Mode 2), before turning the chiller on and utilizing the electrical energy stored in the batteries (operational Mode 3). Besides, since the chiller operates in constant compressor speed (so no capacity modulation in a wide operation range is possible), enough electrical energy should be available from the PV and the batteries before charging the thermal energy storage, in order to avoid grid electricity.

Consequently, a differential battery monitoring controller which controls the state of charge SOC_b was used in order to ensure that the thermal energy storage will be charged only when the battery has reached at least the 75% of its capacity. This controller allows discharging of the battery until the 15% of its capacity, thus defining a minimum depth of discharge (DOD) of 60%. According to the previously described operation of the differential battery monitoring controller, its output signal CS_{BM}, is true when the battery is able to supplementary provide electricity for charging the thermal energy storage. On the other hand, the charging of the thermal energy storage is stopped either when the state of charge of the PCM (SOC) exceeds 95%, or when the state of charge of the battery is lower than 15%. In order to ensure that enough electrical power is available from the PV and minimize the power absorbed by the electricity grid, a check that the output PV power exceeds the 60% of the compressor demand ($P_{PV} > 1.8\ kW_e$) is performed as well prior starting the thermal energy storage charging. As a result the chiller will be ON ($CS_{ext} = 1$), even when no cooling is needed $CS_{TH} = 0$, in order to charge the PCM provided that $CS_{BM} = 1$ and $SOC < 95\%$.

As previously described, when discharging is considered, priority should be given to initially discharging the thermal energy storage. As a result, when cooling is needed ($CS_{TH} = 1$), the VCC should be kept OFF ($CS_{ext} = 0$). This will continue until the thermal energy storage is discharged, which practically was decided to be defined as $SOC < 5\%$, defining a DOD of 90% for the thermal energy storage. Fig. 6 graphically represents what was described above regarding the logical scheme that controls the VCC on/off operation.

3. Simulation results and discussion

Following the detailed description of the modelling approach used for both the simplified vapour compression chiller with the RPW-HEX model development in C++ and the overall HVAC system in TRNSYS, the outcomes from the simulation are presented. Simulations were performed with absolute convergence tolerance of 10^{-4}. First of all, a quick simulation of the thermal energy storage charging and discharging is investigated. Afterwards, the whole system performance is assessed in three different weeks during the start, the mid and the end of the cooling period in Greece, in comparison with the conventional system with no thermal energy storage. Last, the cases of no electrical storage and of better building characteristics (i.e. enhanced insulation) are considered.

3.1. Thermal energy storage charging-discharging test

As previously described, a $10 kWh_{th}$ PCM cooling energy storage was considered in the present study. Given that the nominal capacity of the chiller is around $13\ kW_{th}$, it is estimated that the charging process will last for less than an hour. As a result, for the first 60 min of the simulation, no water flows through the RPW-HEX. In agreement with what was described above, the PCM is considered fully charged once its SOC exceeds the value of 95%, above which the operation of the vapour compression chiller is terminated. Right after the time moment t = 60 min, water begins to circulate inside the RPW-HEX, discharging the storage. Once being fully discharged, the vapour compression chiller is turned ON ($CS_{ext} = 1$) in order to cover the cooling demand. Throughout the simulation the fan coil units TRNSYS models described in the previous section were used as a cooling load, while the temperature of the air entering the coil is assumed constant at 26 °C. The control signal of the fan is the same of the water pump (so it is activated after t = 60 min). For the simulation, a time step of Δt = 10 s was used. Fig. 7 shows the resulted charging and discharging profiles, for various water flow rates, which directly affect the discharge

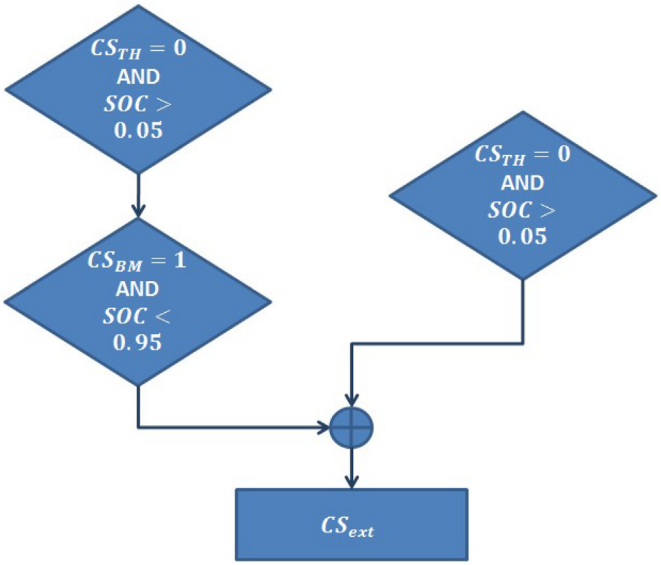

Fig. 6. Hybrid storage system control strategy.

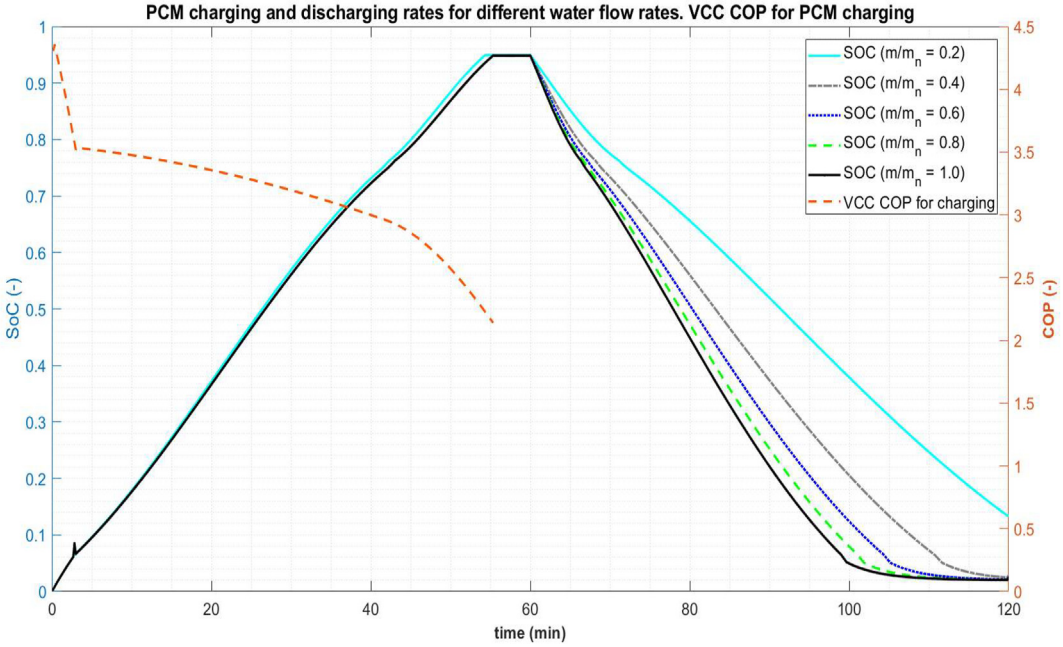

Fig. 7. Charging/discharging test results for the SOC and the COP of the integrated vapour compression chiller RPW-HEX model.

rate. Besides, the COP of the vapour compression chiller during the charging procedure is plotted in order to assess the electrical efficiency of the thermal energy storage charging.

From Fig. 7 it is clear that the discharge rate of the PCM must be controlled in order to effectively utilize the released cooling power, which is in agreement with outcomes of relevant studies [21]. The lower the flow rate, the lower both heat transfer rate in the RPW-HEX. It is clear that in order to obtain a discharging profile similar to the one resulted for charging, the flow rate must be around the half of its nominal value. Besides, this implies reduced capacity of the fan coil units, too, so smoothly discharging the PCM can be ideal during partial load conditions.

Another important aspect is that the COP of the vapour compression chiller is gradually deteriorating during the charging procedure. This can be merely explained by the low evaporating temperatures needed for charging the PCM. This leads to a low efficiency charging of the PCM, which is expected to lead to poor performance compared to the electrical storage (similarly to the results obtained from Ref. [9]), since increased electrical consumption is needed for the same amount of cooling energy.

3.2. Comparative assessment of the system performance

The model of the whole cooling system of the building was simulated for operation with and without thermal energy storage, aiming at the direct comparison between the results of both layouts and the assessment of the performance of the integrated hybrid storage solution and control strategy. In the case with the thermal energy storage, the vapour compression chiller was operating with the RPW-HEX, so the control signal of the solenoid valves was set to $CS_{sv} = 0$, while during the conventional system assessment, the vapour compression chiller was operating using its standard evaporator, so $CS_{sv} = 1$. Due to the high computational cost, the whole system was simulated for three representative weeks in the cooling period (summer) with a time step of $\Delta t = 45s$:

- **Week 1 (W1), June 7**th – **June 14**th**:** It was selected as a period with relatively low cooling demand and moderate solar input
- **Week 2 (W2): July 21**st – **July 28**th**:** It was selected since the highest cooling demands are expected then. The solar input is expected to be high, as well.
- **Week 3 (W3): August 28**th – **September 4**th**:** Moderate cooling demands and solar input are expected; it is a relatively balanced period.

The climate data were acquired from the standard Meteonorm libraries available with the TRNSYS standard package and correspond to the centre of the city of Athens.

Fig. 8 summarizes the cumulative results obtained for the energy absorbed from the electrical grid, E_{grid}, the self-consumption of photovoltaic electricity by the cooling system, E_{sc} and the photovoltaic electricity returned to the grid, E_d. The former two sum to the total energy consumed by the system $E_{load} = \int (P_{comp} + 2 \cdot P_{FCU} + P_{pump}) \cdot dt$, while the latter two sum to the total energy produced by the photovoltaic array ($E_{PV} = \int P_{PV} \cdot dt$). Apart from the total electricity absorbed from the electrical grid, E_{grid}, two more parameters are of primary interest, which are:

- The solar fraction, defined as:

$$SF = \frac{E_{sc}}{E_{grid} + E_{sc}} = \frac{E_{sc}}{E_{load}} \tag{25}$$

- The returned to produced photovoltaic electricity ratio:

$$RPEC = \frac{E_d}{E_{sc} + E_d} = \frac{E_d}{E_{PV}} \tag{26}$$

It is evident that the operation with the thermal energy storage is beneficial for the system, reducing both the grid consumption and the penetration of renewable electricity from the PV for all of the three periods examined. The greatest impact on grid electricity is found for W1, where with the use of thermal energy storage the total consumption drops for about 12.5 kWh_e, while the weakest impact is evident for the W2, where the saved grid electricity is just

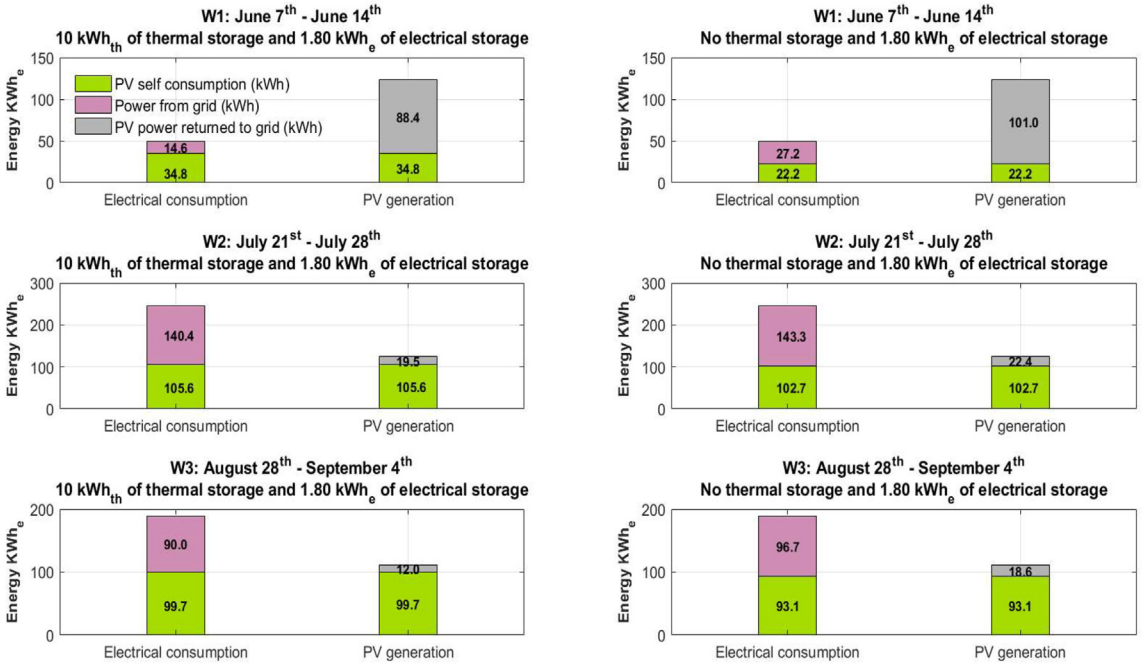

Fig. 8. Cumulative electrical energy results for the hybrid storage layout.

Table 7
Solar fraction and returned to produced photovoltaic electricity ratio for the hybrid storage system.

SF			RPEC	
With PCM		Without PCM	With PCM	Without PCM
W1	0.70	0.45	0.72	0.82
W2	0.43	0.42	0.16	0.18
W3	0.53	0.49	0.11	0.17

3 kW_e, which were both expected since the W1 period is associated with more frequent on/offs of the system, while during W2 the system struggles to cover the cooling demand and the energy storage possibilities are limited. In W3 period, grid energy savings are relatively towards the average of the previous two values, leading to a recovery of 7 kW_e from the sun and a total reduction of the grid electricity of around 7%.

Table 7 summarizes the effect of the thermal energy storage operation on the SF and the RPEC. An enhancement of around 8% is evident during W3 for the SF, while the RPEC is reduced by 37%. RPEC shows a reduction of around 10% for both the W1 and W2 periods as well.

The fact that even if an additional storage solution is utilized, the electricity returned to the grid, E_d, remains greater than zero is an important remark, that primarily shows the lack of flexibility of an on/off control strategy which prevents the adaptation of the system to the variability of the solar energy input. As a result, a lower or even zero value of RPEC is expected if a modulating compression chiller is used in order to charge the thermal energy storage by adapting to the exact value of the available PV electricity, when no cooling is needed.

Fig. 9 presents the profile of the room temperature throughout the W2 period, where the cooling demand is near its maximum. Besides, the response of the state of charge for both the storage systems is also presented.

Even though a small violation of the upper limit temperature is evident for both the systems during July 21st and 22nd (which possibly indicates the need of excess cooling capacity, at least for these two days), the room temperature is strictly inside the limits imposed by the thermostat (except for the hours of the night, when the temperature drops) for both the layouts, even when the thermal energy storage is being discharged. This makes clear that no penalty is imposed in terms of thermal comfort or temperature controllability when the thermal energy storage is utilized. In addition, from the state of charge curves one may notice that the priority of the electrical storage for charging and the priority of the thermal energy storage for discharging, respectively. Besides, it is worth mentioning that the installed PV power is able to charge both storages during the first morning hours.

The above makes clear that the effectiveness of the additional thermal energy storage strongly depend on the cooling demand profile, while it tends to be better (as expected) for partial loads. As a result, it would be really interesting to check the effect of the thermal energy storage operation on a building with lower cooling demands.

3.3. Comparative assessment of the system performance after insulation refurbishment

Based on the previous remark, the system was assessed on the same building, provided that the insulation materials will be upgraded. For reference, the usual refurbishment scenario available in the Tabula Web Tool was utilized, while the total heat loss coefficient is also available in Table 3. Since usually insulation materials have negligible thermal mass, the capacitance of the building was left unchanged.

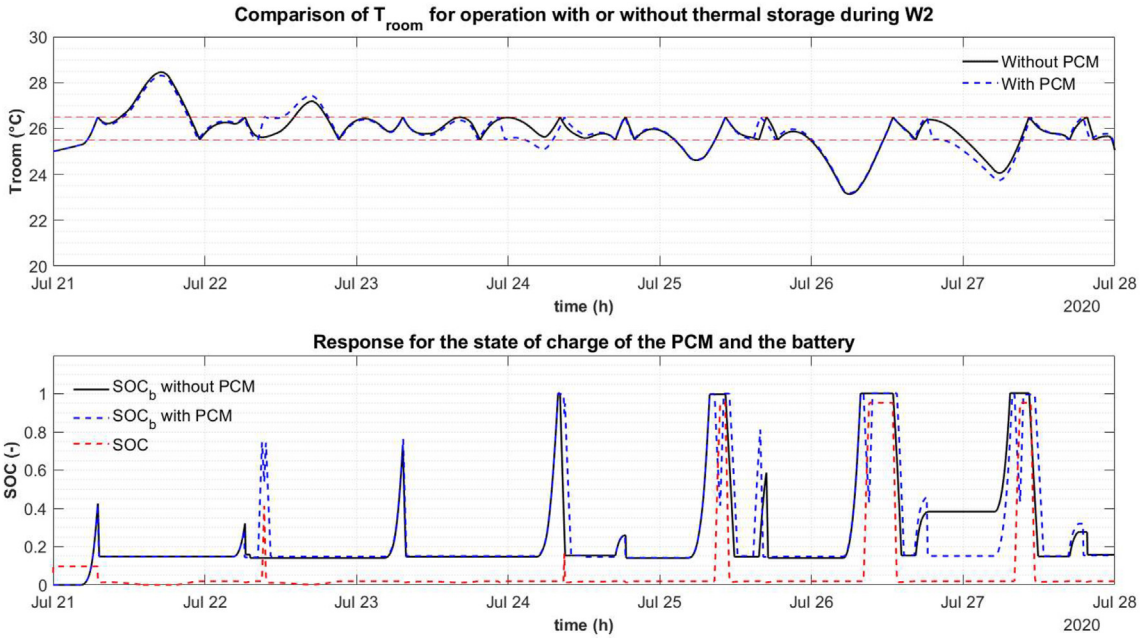

Fig. 9. Room temperature response and storage SOC for the conventional and the hybrid system during W2.

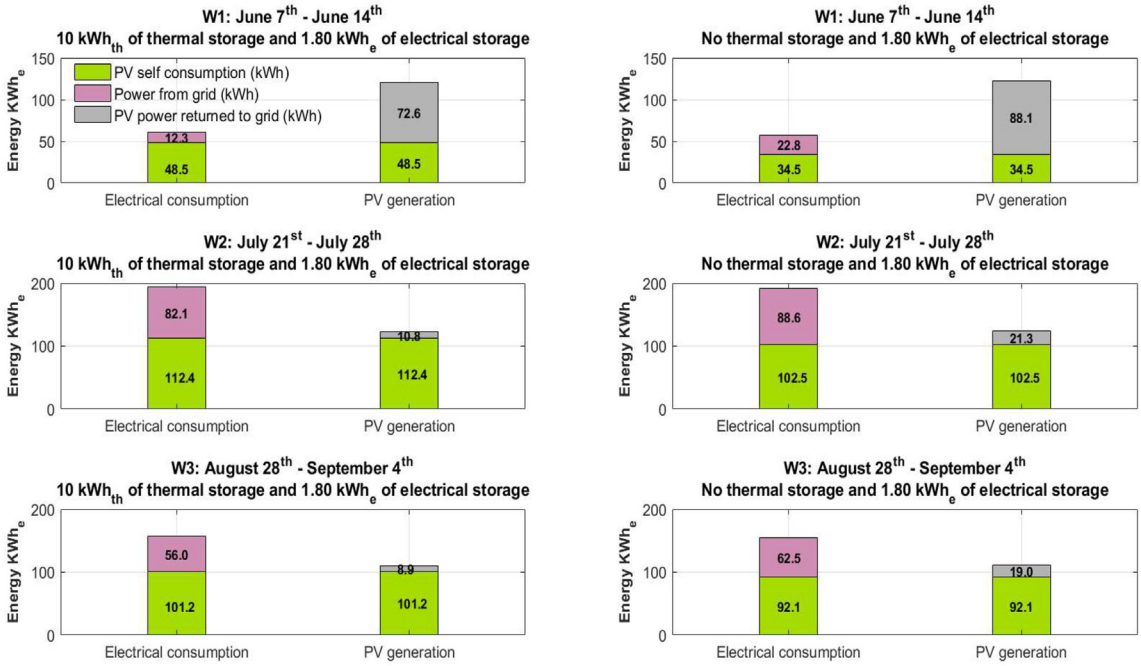

Fig. 10. Cumulative electrical energy results for the hybrid storage layout for reduced cooling demand.

As a result, the new cumulative results for the electrical consumptions are summarized in Fig. 10, while the values for the SF and the RPEC are available in Table 8.

Now the grid electricity savings are (as expected) enhanced in all the examined periods. It is worth mentioning that the grid electricity savings for W2 and W3 are almost identical, reaching the value of 12 kW_e. Besides, important enhancements are evident in the minimization of returned electricity to the grid, since RPEC is reduced from 22% for W1 to 65% for W3 and the SF shows and enhancement of around 13% even for the W2 period.

Table 8
Solar fraction and returned to produced photovoltaic electricity ratio for the hybrid storage system for reduced cooling demand.

Time period	SF		RPEC	
	With PCM	Without PCM	With PCM	Without PCM
W1	0.82	0.58	0.60	0.72
W2	0.58	0.53	0.09	0.17
W3	0.65	0.59	0.08	0.17

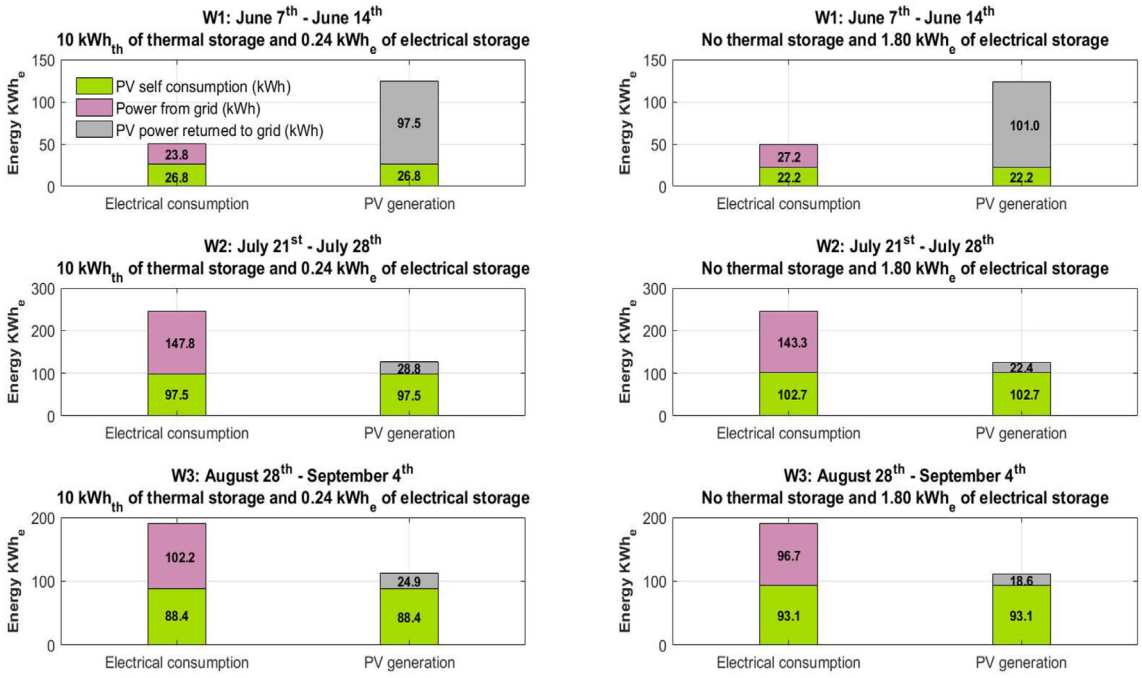

Fig. 11. Cumulative electrical energy results for the conventional system compared to a system equipped only with thermal energy storage.

The above indicate that the installation of thermal energy storage can be proven extremely beneficial for oversized systems, or even for already installed systems in buildings where insulation upgrade is planned to take place.

3.4. Thermal against electrical storage comparison

In order to assess the performance of a PV driven vapour compression chiller with only thermal energy storage, the battery was downsized in order to provide the electrical power needed just for the auxiliary consumptions (i.e. the fan coil units and the pump), based on the same approach as the one followed in the sizing of the hybrid system, ensuring a 40% self-sufficiency. This resulted to a 0.24 kWh_e capacity battery bank, which was operated in parallel with the thermal energy storage based on the hybrid control strategy proposed in the previous section. The cumulative results for the electrical energy are presented in Fig. 11.

It is evident that the performance of the layout based primarily on the thermal energy storage is worse in terms of both electrical energy consumption from the grid and solar fraction, except for the W1 period, where reduced demand is evident (and thus the operating hours of the chiller are less). Actually, this can be explained by the fact that the COP of the chiller when the PCM is charging is significantly worse compared to its nominal value. Besides, since the chiller cannot modulate its power input (since it uses a conventional on/off control), the power consumed by the compressor cannot meet the available power from the PV, resulting in increased consumption from the grid. In terms of RPEC, the difference is not that great, but again indicates that a ratio of PCM storage capacity to battery capacity higher than 6 should be used in order to gain equivalent results for the renewable energy penetration. This, of course, may be changed if the limitation of $P_{PV} > 1.8\ kW_e$ is relaxed, associated with even higher grid electricity consumptions, though.

4. Conclusions

The present study primarily dealt with the development of a simplified model for a vapour compression chiller integrated with a latent heat cold energy storage based on paraffin phase change materials. The conventional evaporator if the chiller was replaced by a novel three fluid heat exchanger filled with refrigerant, the PCM, and water, which made necessary the development of a single integrated model for both the components. The model was developed in C++ for compatibility with the TRNSYS dynamic simulation software and was successfully tested under varying operating conditions, proving numerical stability and robustness.

Using the model in order to simulate the thermal energy storage charging and discharging process, it was found that the COP of the compression chiller drops drastically while the storage is being charged, reaching the value of 2.2 when the storage is fully charged. This directly affects the charging efficiency of the thermal energy storage, leading to a worse performance compared to the usage of batteries for the same cold energy demand. Besides, the results indicated that the water flow rate is an important parameter for controlling the discharge rate of the PCM.

Next, the developed component was added to a conventional photovoltaic driven cooling system (based on vapour compression cooling) simulation flow sheet, which uses conventional lead-acid batteries as storage. As a result, a hybrid storage system combining both the electrical and thermal energy storage solutions was built and simulated, after devising a proper on/off control strategy based. The results were compared against the performance of the conventional system with only electrical storage, indicating enhanced performance and robust operation for the hybrid system. Besides, better performance is expected in case that the on/off strategy is replaced by a cooling capacity modulating system, which of course requires a variable speed compressor for the chiller and a variable flow cooling emission system.

In addition, enhanced performance of the hybrid storage solution is also evident for oversized cooling systems, which may occur in already existing buildings after insulation upgrading, proving the installation of additional energy storage as a competitive efficiency measure.

Last, the comparison of the conventional system with a similar

one, utilizing batteries just for the auxiliary consumptions and replacing the rest of the capacity of the electrical storage with its thermal counterpart, showed a worse performance both in terms of grid electrical consumption and renewable energy penetration, even though slightly better performance was evident only during W1, which is associated with reduced cooling demand. These results were attributed to the lack of a power modulating chiller, capable to follow the variability of the solar energy input and the worse COP of the chiller during the PCM charging.

In any case, the installation of batteries instead of thermal storage is always an option, even for the hybrid scenarios tested. Of course, apart from the energetic assessment, life cycle assessment (LCA) and life cycle cost (LCC) analyses of the competitive systems should be carried out before concluding which one is the best solution.

CRediT authorship contribution statement

Efstratios Varvagiannis: developed the custom TRNSYS type of the compression chiller along with the RPW-HEX as well as the TRNSYS simulation flowsheet of the thermal part of the system. **Antonios Charalampidis:** developed the electrical part of the simulation flowsheet in TRNSYS. **Gabriel Zsembinszki:** Writing - review & editing, developed the simplified model of the RPW-HEX and revised the paper. **Sotirios Karellas:** Writing - original draft, wrote the paperand. **Luisa F. Cabeza:** Writing - original draft, wrote the paper.

Declaration of competing interest

The authors declare that they have no known competing financial interests or personal relationships that could have appeared to influence the work reported in this paper.

Acknowledgements

This study has received funding from the European Union's Horizon 2020 research and innovation programme under grant agreement No 768824. This work was partially funded by the Ministerio de Ciencia, Innovación y Universidades de España (RTI2018-093849-B-C31). The authors would like to thank the Catalan Government for the quality accreditation given to their research group (2017 SGR 1537). GREiA is certified agent TECNIO in the category of technology developers from the Government of Catalonia. This work is partially supported by ICREA under the ICREA Academia programme.

References

[1] The European parliament and the council of the European union, "directive 2012/27/EU OF the EUROPEAN parliament and OF the council,", *Off.* J. Eur. Union (2012) 1–56. October 2012.
[2] European Comission, EU Energy in Figures, Statistical Pocketbook, 2018.
[3] The European Parliament and the Council of the European Union, "DIRECTIVE 2010/31/EU OF the EUROPEAN parliament and OF the council,", *Off.* J. Eur. Union (2010) 13–35.
[4] P. Pallis, et al., Cost effectiveness assessment and beyond: a study on energy efficiency interventions in Greek residential building stock, Energy Build. 182 (2019).
[5] R.M. Lazzarin, "Solar cooling : PV or thermal ? A thermodynamic and economical analysis Refroidissement solaire : photovoltaïque ou thermique ? ' conomique Analyse thermodynamique et e, Int. J. Refrig. 39 (2013) 38–47.
[6] T. Otanicar, R.A. Taylor, P.E. Phelan, "Prospects for solar cooling – an economic and environmental assessment, Sol. Energy 86 (5) (2012) 1287–1299.
[7] M. Beck, K. Müller, W. Arlt, Storing surplus solar energy in low temperature thermal storage for refrigeration applications, Energy Build. 122 (2016) 192–198.
[8] Z. Wu, D. Pan, N. Gao, T. Zhu, F. Xie, Experimental testing and numerical simulation of scroll expander in a small scale organic Rankine cycle system, Appl. Therm. Eng. 87 (2015) 529–537.
[9] X. Wang, M. Dennis, Influencing factors on the energy saving performance of battery storage and phase change cold storage in a PV cooling system, Energy Build. 107 (2015) 84–92.
[10] V. Dermardiros, Y. Chen, A.K. Athienitis, Modelling of an active PCM thermal energy storage for control applications, in *6th International Building Physics Conference* 78 (2015) 1690–1695.
[11] J. Sa, A.J. Gallego, L.F. Cabeza, E.F. Camacho, E. Oro, Mathematical modeling of a PCM storage tank in a solar cooling plant, Sol. Energy 93 (2013) 1–10.
[12] W. Stoecker, J. Jones, Refrigeration and Air Conditioning, second ed., McGraw-Hill, 1983.
[13] F. Incropera, D. De Witt, F. Bergman, and A. Lavine, Fundamentals of Heat and Mass Transfer, seventh ed. Wiley.
[14] C.A. Balaras, A.G. Gaglia, E. Georgopoulou, S. Mirasgedis, Y. Sarafidis, D.P. Lalas, European residential buildings and empirical assessment of the Hellenic building stock , energy consumption , emissions and potential energy savings, Build. Environ. 42 (2007) 1298–1314.
[15] "TABULA Web Tool." [online], Available: http://webtool.building-typology.eu/#bm. (Accessed 23 February 2019).
[16] Technical Chamber of Greece, "Analytical National Specifications of the Parameters for the Calculation of the Building Energy Performance and Issuing of Energy Certificates, 2017.
[17] W. De Soto, S.A. Klein, W.A. Beckman, Improvement and validation of a model for photovoltaic array performance, Sol. Energy 80 (2006) 78–88.
[18] U. Eicker, Solar Technologies for Buildings, first ed., Wiley, 2003.
[19] D. Serrano, Quantum Cutting Processes in Rare-Earth Doped Fluorides for Photovoltaic Quantum Cutting Processes in Rare-Earth Doped Fluorides for Photovoltaic Applications, University of Caen, 2015.
[20] J. Weniger, T. Tjaden, V. Quaschning, "Sizing of residential PV battery systems sizing of residential PV battery systems,", Energy Procedia 46 (2014) 78–87. June 2016.
[21] X. Li, D. Qu, L. Yang, K. Li, Experimental and numerical investigation of discharging process of direct contact thermal energy storage for use in conventional air-conditioning systems, Appl. Energy 189 (2017) 211–220.

Nomenclature

Symbols

A: area, m^2
c_p*:* specific heat, kJ/kgK
e: efficiency,
E: energy, kJ
h: convective heat transfer coefficient, W/m^2K
m: mass flow, kg/s
P: power, kW_{el}
Q: heat flow (>0 when heat is released, in order to indicate cooling generation), kW_{th}
T: temperature, °C
t: time, s
U: overall heat transfer coefficient, W/m^2K
V: volume, m^3
ε*:* effectiveness of HEX,
λ*:* thermal conductivity, W/mK
ρ*:* density, kg/m^3

Subscripts

b: batteries
BM: battery manager
comp: compressor
d: dumped
evap: evaporation
ext: External
grid: to/from grid
mot: motor
nom: nominal
pcm: phase change material
PV: from photovoltaics
r: eefrigerant
SC: self-consumed
SP: set-point
std: standard
TH: thermostat
w: water
wc: condenser water
we: evaporator water

Abbreviations

COP: Coefficient of Performance
CS: Control Signal

EU: European Union
FCU: Fan Coil Unit
HEX: Heat Exchanger
HTF: Heat Transfer Fluid
NTU: Number of Transfer Units
PCM: Phase Change Material
PV: Photovoltaics
RPEC: Returned to Produced Electricity Ratio
RPW: Refrigerant-PCM-Water
SF: Solar Fraction
SOC: State of Charge